



High-silica faujasite zeolite-tailored metal encapsulation for the low-temperature production of pentanoic biofuels

Wenhao Cui^{a,b,1}, Yuanshuai Liu^{c,1}, Pengfei Guo^d, Zhijie Wu^e, Liqun Kang^f, Huawei Geng^c, Shengqi Chu^g, Linying Wang^a, Dong Fan^a, Zhenghao Jia^h, Haifeng Qiⁱ, Wenhao Luo^{d,*}, Peng Tian^{a,*}, Zhongmin Liu^{a,*}

^a National Engineering Research Center of Lower-Carbon Catalysis Technology, Dalian National Laboratory for Clean Energy, Dalian Institute of Chemical Physics, Chinese Academy of Sciences, Dalian 116023, Liaoning, China

^b University of Chinese Academy of Sciences, Beijing 100049, China

^c Qingdao Institute of Bioenergy and Bioprocess Technology, Chinese Academy of Sciences, Qingdao 266101, Shandong, China

^d College of Chemistry and Chemical Engineering, Inner Mongolia University, Hohhot 010021, Inner Mongolia, China

^e State Key Laboratory of Heavy Oil Processing and Key Laboratory of Catalysis of CNPC, China University of Petroleum, Beijing 102249, China

^f Department of Inorganic Spectroscopy, Max Planck Institute for Chemical Energy Conversion, Mülheim an der Ruhr 45470, Germany

^g Beijing Synchrotron Radiation Facility, Institute of High Energy Physics, Chinese Academy of Sciences, Beijing 100049, China

^h Division of Energy Research Resources, Dalian Institute of Chemical Physics, Chinese Academy of Sciences, Dalian 116023, Liaoning, China

ⁱ Leibniz-Institut für Katalyse, Albert-Einstein-Straße 29a, Rostock 18059, Germany

ARTICLE INFO

Article history:

Received 11 September 2023

Revised 6 October 2023

Accepted 7 October 2023

Available online 17 October 2023

Keywords:

High-silica zeolite Y
Metal encapsulation
Bifunctional catalysis
Hydrodeoxygenation
Biofuels

ABSTRACT

Zeolite-encapsulated metal nanoclusters are at the heart of bifunctional catalysts, which hold great potential for petrochemical conversion and the emerging sustainable biorefineries. Nevertheless, efficient encapsulation of metal nanoclusters into a high-silica zeolite Y in particular with good structural integrity still remains a significant challenge. Herein, we have constructed Ru nanoclusters (~1 nm) encapsulated inside a high-silica zeolite Y (SY) with a SiO₂/Al₂O₃ ratio (SAR) of 10 via a cooperative strategy for direct zeolite synthesis and a consecutive impregnation for metal encapsulation. Compared with the benchmark Ru/H-USY and other analogues, the as-prepared Ru/H-SY markedly boosts the yields of pentanoic biofuels and stability in the direct hydrodeoxygenation of biomass-derived levulinic acid even at a mild temperature of 180 °C, which are attributed to the notable stabilization of transition states by the enhanced acid accessibility and properly sized constraints of zeolite cavities owing to the good structural integrity.

© 2023 Science Press and Dalian Institute of Chemical Physics, Chinese Academy of Sciences. Published by ELSEVIER B.V. and Science Press. All rights reserved.

1. Introduction

Zeolites are a class of crystalline materials with paramount importance to the chemical industries [1,2]. Their well-defined microporous architectures, tunable acidity, and functional sites render them the catalytic workhorses of various reactions in petrochemical refineries [3–5]. Additionally, zeolites have been shown to be powerful and attractive scaffolds for immobilizing small metal entities to generate efficient bifunctional catalysts [6–9]. In particular, the encapsulation of metal particles inside the cavities of zeolites, which could efficiently prevent the agglomeration and leaching of metal species due to the spatial confinement of micro-

porous structures, offers an efficient approach for achieving ultra-fine and well-dispersed metal species with excellent (hydro)thermal stability [7,10–12]. Besides, metal encapsulation in well-defined microporous architecture of zeolites can provide sites proximity between acid and metal sites, which could enhance catalytic performance in terms of activity and selectivity due to inducing synergistic effects between functional sites within confined microenvironments [13–19]. In view of those advantages in catalytic performance, zeolite-encapsulated metal catalysts have attracted considerable attention in both academia and industry, which further stimulates an extensive interest in rational design and understanding of such zeolitic bifunctional materials in numerous heterogeneous catalytic processes [20–23].

Zeolite Y, which possesses the FAU topology with three-dimensional 12-membered ring channels and nanosized supercages, is one of the most widely-applied zeolites, which excels in catalytic performance in various important petrochemical applica-

* Corresponding authors.

E-mail addresses: w.luo@imu.edu.cn (W. Luo), tianpeng@dicp.ac.cn (P. Tian), zml@dicp.ac.cn (Z. Liu).

¹ These authors contributed equally to this work.

tions, such as (hydro)cracking and the fluid catalytic cracking (FCC) [24]. Besides, FAU-type zeolitic catalysts recently show a promising potential in decarbonization of the energy and the transportation sector for a circular economy offered by the emerging sustainable valorization of biomass sources and plastic wastes [13,25]. Nevertheless, the high framework Al content of FAU-type zeolites could bring primary challenges in hydrothermal stability and acid strength which thus interferes their catalytic performance. Although various post-modification approaches, including hydrothermal dealumination and fluoride etching, have been employed for removing partial framework Al species, those iterative treatments in acid or alkaline solutions, which are often time-consuming and energy-intensive, could lead to a loss of crystallinity and generation of defects and extra-framework species [26–29]. In view of this, the direct synthesis of high-silica zeolite Y has attracted significant attention recently [6,30,31] owing to the enhanced (hydro)thermal stability and acid accessibility, which would facilitate their catalytic application. Further combining encapsulation of metal clusters in the cavities of high-silica FAU framework is of great significance and interest in material design and catalysis, which has been rarely reported to date.

Hydrodeoxygenation (HDO) is one of the key reactions involved in biomass valorization [32–34], which generally includes a combination of hydrolysis, dehydration, and hydrogenation steps, and preferably requires both metal and acid functionalities in one catalyst for efficiently coupling different reaction steps. Currently, bifunctional zeolite-encapsulated metal catalysts are being quite extensively studied for the HDO of biomass and its platform molecules [10,14,15,32]. Of particular interest is the utilization of biomass-derived platform molecules for transportation fuels production with the aim of reducing their reliance on fossil resources. Among all the promising biofuel candidates, pentanoic biofuels, derived from levulinic acid or levulinates, are in the spotlight owing to their excellent fuel property and good compatibility with combustion engine [35]. Recent work demonstrated that Ru clusters encapsulated in the cavities of a commercial FAU-type zeolite could provide sites proximity between acid and metal sites, which played a crucial role in the improved activity and selectivity for the production of pentanoic biofuels at 220 °C [16]. However, there is still a strong need to develop efficient bifunctional catalysts with superior HDO performance, in particular for operating catalysts under more demanding mild temperatures for alleviating the thermo-severeness and thus improving catalyst durability.

In this work, well-dispersed Ru nanoclusters (~1 nm) confined inside the cavities of high-silica FAU zeolite with a SAR of 10 and good framework integrity have been developed for the first time by a cooperative strategy for zeolite synthesis and an improved wet impregnation method for metal encapsulation (details shown in Supporting Information, SI). For comparison, a Ru/H-USY with commercial high-silica USY (SAR = 10) as the support has been prepared and used as a benchmark catalyst. The HDO performance of the two bifunctional catalysts is assessed for the production of pentanoic biofuels. The Ru/H-SY catalyst can afford an enhanced catalytic activity and stability in HDO of neat methyl levulinate into pentanoic biofuels even at a mild temperature of 180 °C. The superior catalytic performance of Ru/H-SY was investigated by a combination of scanning transmission electron microscopy (STEM), integrated differential phase-contrast (iDPC) STEM, X-ray absorption spectroscopy (XAS), Fourier transform infrared spectroscopy (FT-IR), and ²⁷Al magic angle spin nuclear magnetic resonance (MAS NMR) spectroscopy. On the basis of detailed characterizations and kinetic studies, the enhanced catalytic performance has, therefore, been attributed to the notable stabilization of transition states by the enhanced acid sites accessibility, confined sites proximity, and properly sized constraints of zeolite

pores due to the successful metal encapsulation and the good integrity of zeolite structure.

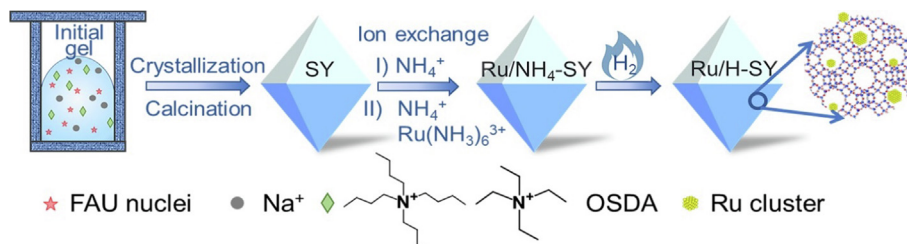
2. Results and discussion

The preparation strategy for the high-silica zeolite Y (SY) encapsulated Ru clusters has been illustrated in Scheme 1. Zeolite SY was directly synthesized by a cooperation strategy, which involves the use of FAU nuclei solution, tetrabutylammonium hydroxide template, and a low alkalinity gel system [6]. Subsequently, the calcined SY was converted to the ammonium form by an ion-exchange method. The utilization of ammonium-form zeolite to immobilize metal species could facilitate their encapsulation in the zeolite cavities, preserve strong acid sites, and improve the metal-acid site proximity at a sub-nanoscale [36]. Specifically, Ru/H-SY was prepared using a cationic complex of Ru(NH₃)₆³⁺ as precursor via an improved wet impregnation method, in which the high-temperature calcination in air was omitted. The following H₂ reduction was applied to decompose the Ru precursor and convert ammonium-form zeolite to H-form analogue. For comparison, Ru clusters encapsulated inside a commercial USY zeolite were also prepared as the benchmark catalyst via the same deposition method.

The X-ray diffraction (XRD) patterns of H-SY, Ru/H-SY, H-USY, and Ru/H-USY samples present characteristic peaks belonging to the FAU topology (Fig. S1). No peaks corresponding to Ru phases can be observed, indicating the absence of large Ru particles in Ru/H-SY and Ru/H-USY. Intriguingly, a close inspection of XRD patterns reveals that Ru/H-SY possesses a higher crystallinity than Ru/H-USY, implying the better structural integrity of Ru/H-SY. The elemental compositions, textural properties, metal dispersions, and particle sizes of the samples are given in Table S1. All samples have a similar SAR of 10, as measured by X-ray fluorescence (XRF). The Ru content of both Ru-containing samples is determined to be ~1 wt% by inductively coupled plasma optical emission spectrometer (ICP-OES). In Fig. S2, both H-SY and Ru/H-SY present a typical type-I isotherm, indicating the dominance of microporosity, while H-USY and Ru/H-USY give a type-IV isotherm with a large H4 hysteresis loop, suggesting the existence of both mesopores and micropores. This is in line with the scanning electron microscope (SEM) results (Fig. S3) that Ru/H-USY exhibits a sponge-like morphology as a result of dealumination during the preparation of USY. Compared with Ru/H-USY, Ru/H-SY possesses an obviously larger micropore area and micropore volume, consistent with its good crystallinity and structural integrity.

Aberration-corrected STEM (AC-STEM) and the corresponding energy-dispersive X-ray (EDX) spectroscopy were conducted to characterize the metal dispersion on Ru/H-SY and Ru/H-USY (Fig. 1a–f). Analyses of high-angle annular dark-field (HAADF) images reveal that the Ru clusters are highly dispersed and uniformly distributed in both samples with average size of ~1.5 nm, indicating the successful Ru encapsulation inside the cavities of zeolites by this simple preparation approach. EDX-mapping analysis corroborates the homogeneous distribution of well-defined Ru nanoclusters in the crystals. Moreover, CO chemisorption results (Table S1) show an average metal cluster size of slightly smaller than 1.5 nm for Ru/H-SY and Ru/H-USY, again confirming the highly dispersed Ru clusters (*D* >75%) encapsulated inside both zeolitic materials.

To further validate the spatial distribution of Ru clusters inside zeolites, iDPC-STEM is employed to achieve atomic-resolution images of beam-sensitive zeolitic materials [37–40]. We first perform the low-dose iDPC-STEM measurements for the parent H-SY (Fig. 1g and Fig. S4). Clearly, the iDPC-STEM images of H-SY show a crystal structure with an ordered micropore size of ~0.8 nm,



Scheme 1. Schematic illustration for the preparation approach for the encapsulation of Ru nanoclusters in high-silica zeolite SY.

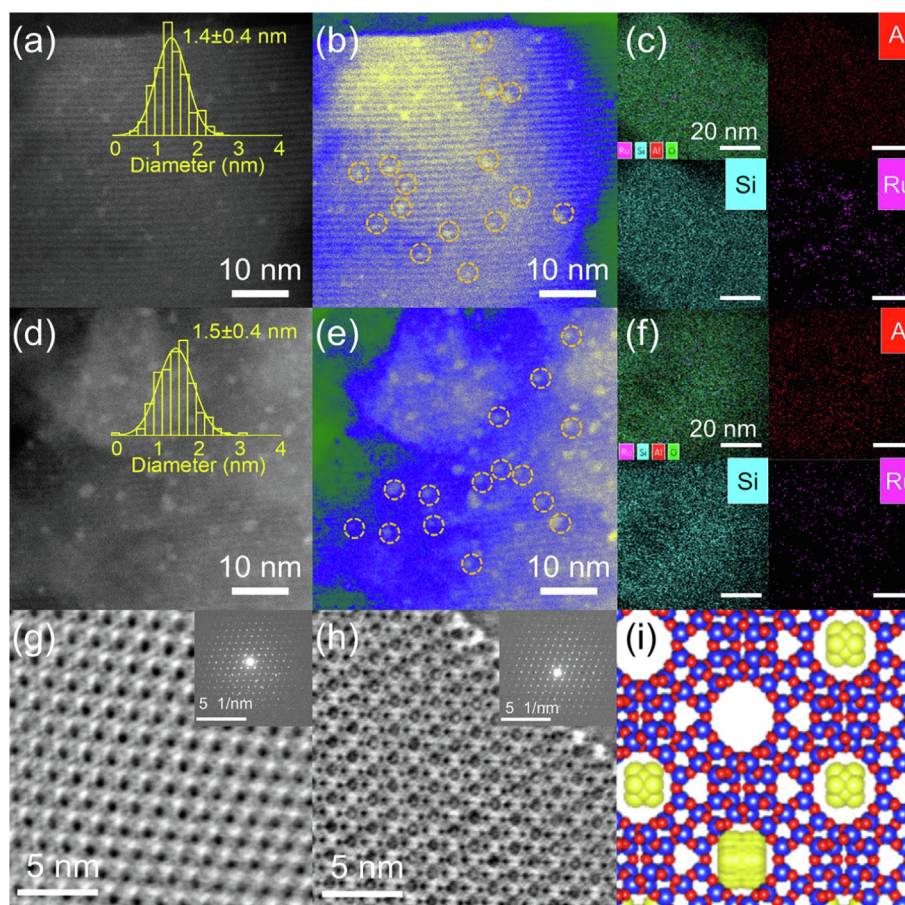


Fig. 1. HADDF-STEM images and EDX spectral images of (a–c) Ru/H-SY and (d–f) Ru/H-USY. iDPC-STEM images and corresponding FFT patterns of the (110) projection of (g) H-SY and (h) Ru/H-SY. (i) The structural model of FAU framework of Ru/H-SY. The cluster size distributions in (a and d) were derived from measurements of over 200 particles. Pretreatment condition for (g and h): vacuum drying (10^{-3} Pa) at 150 °C for 30 min to remove adsorbents in zeolite.

and the corresponding fast Fourier transform (FFT) pattern reflects a high degree of crystallinity along the projected (010) direction, confirming the good integrity of the FAU structure. No apparent guest species can be visualized for H-SY after the vacuum drying treatment. Interestingly, ultra-small Ru clusters located inside the zeolite channels can be directly visualized for Ru/H-SY (Fig. 1h and Fig. S4). This reinforces the substantial amount of ultrasmall Ru clusters encapsulated inside the cavities of H-SY [38]. The above characterizations indicate that this improved wet impregnation method is effective for realizing the encapsulation of small Ru clusters. Compared with in situ encapsulation strategy, this separate Ru deposition can avoid the disadvantageous impact of metal precursors on the assembly of zeolite frameworks and realize homogeneous dispersion of metal clusters in the zeolites. Such a metal-zeolite combination with well-dispersed Ru clusters encapsulated inside a high-silica FAU framework could possess

many advantages such as enhanced (hydro)thermal stability, zeolite crystallinity, and high density of strong acid sites, thus leading to remarkable catalytic performance.

The acid properties provided by zeolite microenvironments play a pivotal role in constructing the metal-acid sites intimacy confined in the zeolite cavities, which is crucial for tailoring the catalytic performance. The acid properties of the samples were characterized by temperature-programmed desorption of ammonia (NH_3 -TPD), FT-IR and solid state NMR spectroscopy. The NH_3 -TPD results (Fig. 2a) show that Ru/H-SY possesses more acid sites, in particular strong acid sites, than Ru/H-USY. This agrees with previous reports that the high-silica SY has a larger concentration of strong acid sites than the USY with similar SAR [6]. The evaluated acid sites amounts of the catalysts based on the deconvoluted NH_3 -TPD curves are displayed in Table S2. Fig. 2(b) gives the FT-IR spectra of adsorbed pyridine (FT-IR-Py). The absorption bands at 1542

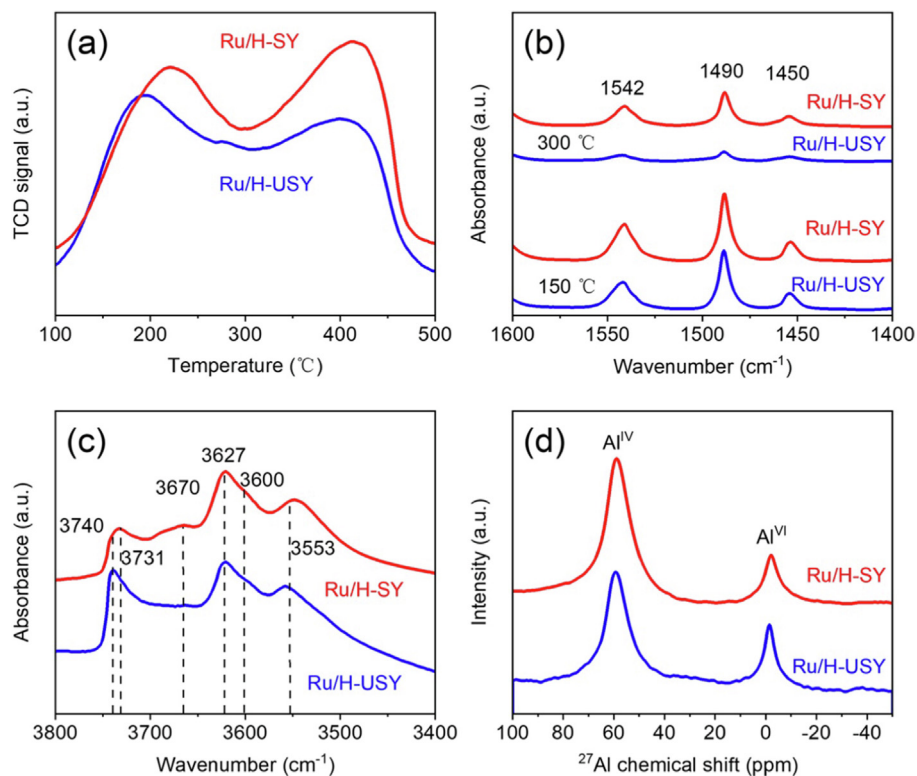


Fig. 2. (a) NH_3 -TPD profiles. (b) FT-IR spectra of pyridine ring-related vibration regions after pyridine desorption at 150 and 300 °C. (c) FT-IR spectra of the hydroxyl stretching region. (d) ^{27}Al MAS NMR spectra of Ru/H-SY and Ru/H-USY.

and 1450 cm^{-1} are characteristic of pyridine coordinated with Brønsted acid sites (BAS) and Lewis acid sites (LAS), respectively [41]. Clearly, both catalysts have higher amount of BAS rather than LAS. Moreover, the BAS amount on Ru/H-SY is larger than that on Ru/H-USY, which is more apparent after pyridine desorption at 300 °C.

The FT-IR spectra of the hydroxyl stretching region for Ru/H-SY and Ru/H-USY are shown in Fig. 2(c). The signals at 3740 and 3731 cm^{-1} are attributed to terminal silanols located at the external surface and the internal surface, respectively. The signals at 3670 and 3600 cm^{-1} are due to hydroxyls linked to extra-framework aluminum (EFAl) species. The signals at 3627 and 3553 cm^{-1} correspond to BAS located in the supercages and the sodalite cages, respectively [42]. In comparison with Ru/H-USY, Ru/H-SY shows higher signal intensities at 3627 and 3550 cm^{-1} , indicating a larger amount of BAS in Ru/H-SY, which is in line with the FT-IR-Py results. Besides, the relatively weak vibration of terminal silanols for Ru/H-SY implies its good structural integrity, in line with XRD and N_2 physisorption results.

The ^{27}Al MAS NMR spectra of the samples are depicted in Fig. 2(d). The signal around 59 ppm is assigned to tetrahedral framework aluminum (FAI^{IV}), while that at ca. 0 ppm is associated with octahedral EFAl species [43,44]. Ru/H-SY exhibits a FAI^{IV} of 84% and an EFAl of 16%. Ru/H-USY gives a FAI^{IV} of 71% and an EFAl of 29% (Fig. S5). The higher proportion of FAI^{IV} in Ru/H-SY, in good accordance with the larger amount of BAS and strong acid sites detected by NH_3 -TPD and FT-IR-Py, reflects that the formation of EFAl during the catalyst preparation can be efficiently suppressed. The ^{29}Si MAS NMR spectra of the samples are shown in Fig. S6. The framework SAR of Ru/H-SY and Ru/H-USY can thus be calculated to be 13 and 18 respectively, which are higher than those determined by XRF and consistent with the existence of EFAl revealed by ^{27}Al spectra. Obviously, Ru/H-SY possesses advantages in acid concentration especially in the strong acid sites compared to Ru/

H-USY, owing to its well-preserved crystallinity and good integrity of zeolite structure.

To verify whether the local structures visualized by AC-STEM are representative for the entirety of the materials, Ru-containing zeolites were further characterized by XAS, which also provide the information about the coordination and local chemical environment of Ru species. The results are displayed in Fig. 3(a and b), Fig. S7, and Table S3. Ru/H-SY and Ru/H-USY have a comparable valence state of $\text{Ru}^{\delta+}$ (bearing a slightly positive charge) and coordination of Ru. The chemical valence of Ru in Ru/H-SY is slightly higher than that in Ru/H-USY. This is in line with the X-ray photoelectron spectroscopy (XPS) results (Fig. S8), indicating a stronger interaction between zeolite framework and encapsulated metal clusters owing to the tight confines of the good structural integrity. Fourier transforms of the corresponding extended X-ray absorption fine structure (EXAFS) reveal two well-defined coordination shells at ~ 1.99 and 2.69 \AA for both samples with Ru–O and Ru–Ru scattering contributions, respectively. The relatively low coordination number (CN) of Ru–Ru and higher CN of Ru–O for both Ru/H-SY ($\text{CN}_{\text{Ru–Ru}} = 3.2 \pm 0.5$, $\text{CN}_{\text{Ru–O}} = 4.7 \pm 0.5$) and Ru/H-USY ($\text{CN}_{\text{Ru–Ru}} = 3.8 \pm 0.8$, $\text{CN}_{\text{Ru–O}} = 5.1 \pm 1.0$), as compared to the standard Ru foil ($\text{CN}_{\text{Ru–Ru}} = 12$, $\text{CN}_{\text{Ru–O}} = 0$), corroborate the formation of ultra-small Ru clusters [13,45]. Similar values of $\text{CN}_{\text{Ru–Ru}}$ and $\text{CN}_{\text{Ru–O}}$ were reported for TiO_2 or zeolite Y supported Ru clusters, due to the existence of dominant Ru sub-nanometric species [46]. Thus, the XAS results corroborate the substantial fraction of Ru nanoclusters in the entirety of Ru/H-SY and Ru/H-USY.

FT-IR spectra of CO adsorption on the samples were performed at -170 °C with a gradual increment of CO pressure from 25 to 300 Pa (Fig. 3c and d). Both Ru/H-SY and Ru/H-USY display the development of peaks at around 2177, 2130, 2040/2032, and 1875 cm^{-1} , which correspond to CO adsorbed on the protons of the zeolites, multi-coordinated Ru^{n+} -CO, linear $\text{Ru}^{\delta+}$ -CO and bridging Ru–CO–Ru, respectively [15,46–51]. The comparable signal

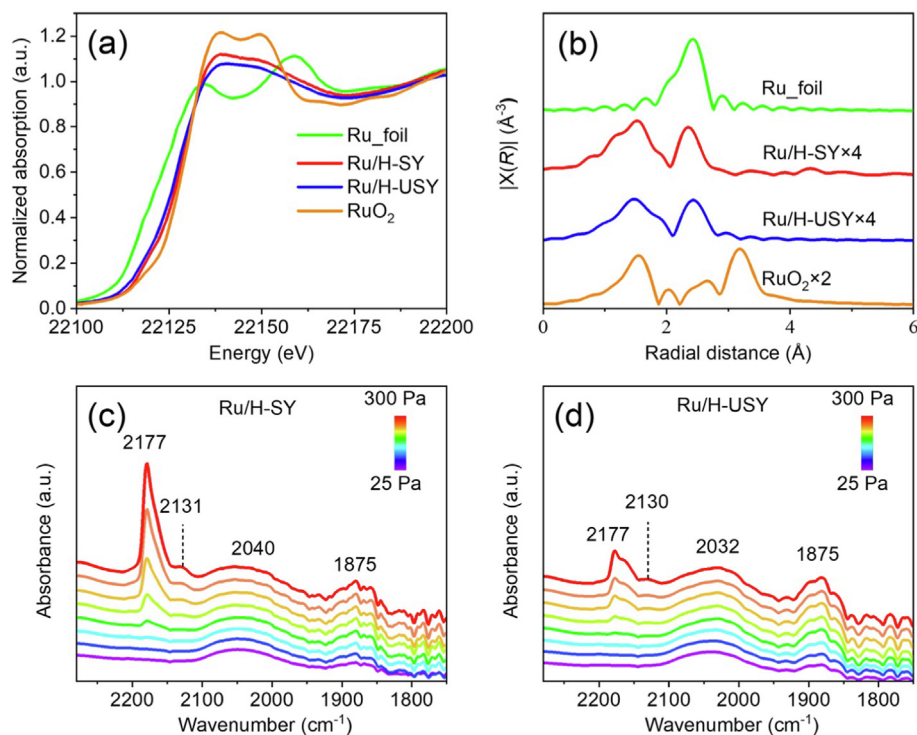


Fig. 3. (a) Normalized Ru K-edge XANES and (b) Fourier transforms of the k^2 -weighted EXAFS of Ru/H-SY, Ru/H-USY, and reference materials. (c, d) FT-IR spectra of CO adsorption on Ru/H-SY and Ru/H-USY at -170 °C with different CO pressures.

pattern of Ru species indicates that they exist as clusters bearing a slightly positive charge for both samples. Notably, a positive shift of linear $\text{Ru}^{\delta+}\text{-CO}$ (8 cm^{-1}) signals can be discerned for Ru/H-SY comparing with that for Ru/H-USY. This indicates that the encapsulated Ru species inside the H-SY bear a slightly positive charge, due to the induced electronic interactions between the confined Ru species and zeolitic frameworks. This is also supported by H_2 temperature programmed reduction [13,52] (H_2 -TPR, Fig. S9) and in line with XAS and XPS results. Besides, Ru/H-SY shows a higher peak intensity of $\sim 2177\text{ cm}^{-1}$ than Ru/H-USY, indicating an enhanced accessibility of acid sites. This is consistent with the results of various acid characterization performed in this study, such as NH_3 -TPD, FT-IR-Py, FT-IR of the hydroxyl stretching region and ^{27}Al MAS NMR.

Engineering the metal-acid sites proximity by encapsulating metal nanoclusters in zeolite cavities could bring benefits and even synergistic effect in the biomass-related HDO transformations [13–16]. We employed neat methyl levulinate (ML) as the substrate to assess the HDO performance of Ru/H-SY and Ru/H-USY under batch conditions at $160\text{--}200$ °C and 40 bar H_2 (Fig. S10). Although a higher reaction temperature can result in many side reactions which in turn decrease the selectivity of target products, a certain threshold reaction temperature of ≥ 220 °C is normally required to achieve an appreciable activity and selectivity towards deep HDO products, such as pentanoic acid and its ester (PA/MP). Remarkably, at a relatively low temperature of 180 °C, Ru/H-SY could afford nearly complete conversion of ML together with a high yield of PA/MP ($\sim 75\%$) after 6 h. A series of Ru-zeolite combination catalysts (Ru/H-USY, Ru/La-Y, and the mixtures of zeolites and Ru nanoclusters, such as Ru/ SiO_2 + H-SY and Ru/ SiO_2 + H-USY) have been rationally assessed and compared under the identical conditions (Fig. 4a). Ru/H-USY and Ru/La-Y, with the confined metal-acid sites proximity, show a complete conversion of ML and a PA/MP yield of $\sim 30\%$, while the mixtures of Ru/ SiO_2 and different zeolites give an inferior performance in terms of both activity

and PA/MP selectivity. Notably, Ru/H-SY shows at least a two-fold increase in PA/MP yield at 180 °C compared with other Ru-based heterogeneous catalysts. Those results are in good line with previous reports that zeolite-tailored active sites proximity could indeed enhance the performance in the one-pot HDO of levulinic acid into pentanoic biofuels [13] and other biomass-derived platform molecules [14–16]. To date, such an enhancement of deep HDO capacity on Ru/H-SY is hitherto unattained over metal/zeolite catalysts at such a low reaction temperature of 180 °C.

Based on the time profiles shown in Fig. 4(b and c), the productivities of PA/MP are determined to be $5.021\text{ mol g}_{\text{Ru}}^{-1}\text{ h}^{-1}$ for Ru/H-SY and $2.720\text{ mol g}_{\text{Ru}}^{-1}\text{ h}^{-1}$ for Ru/H-USY respectively. Compared with the previous reported Ru/La-Y [13], Ru/H-USY affords a similar level of the PA/MP productivity. Although Ru/H-USY shows a faster conversion rate of ML at the initial reaction time, γ -valerolactone (GVL) dominates in the product distribution ($>75\%$) over time at this fairly low reaction temperature of 180 °C. Ru/H-SY shows an enhanced yield of PA/MP as the reaction proceeds, indicating a unique HDO ability for pentanoic biofuels production. Such an improved yield of PA/MP and a high PA/MP productivity especially at a relatively mild temperature of 180 °C, to our knowledge, are seldomly achieved for the direct HDO of levulinic acid.

The reusability of the catalysts is studied by carrying out consecutive tests in the direct HDO of ML into PA/MP (Fig. 4d and e). For Ru/H-SY, no apparent decrease in activity and selectivity could be found even after five cycle runs. The ML conversion and PA/MP yield can sustain at $\sim 77\%$ and $\sim 21\%$ respectively in the fifth run, evidencing a good stability of Ru/H-SY. In contrast, an obvious deactivation is observed for Ru/H-USY, with an apparent decrease in ML conversion from 91% to 60% and PA/MP yield from 16% to 2% upon five consecutive runs. Through the characterization of the spent catalysts (Fig. S11 and Table S1), metal agglomeration and zeolite deconstruction are evidenced for Ru/H-USY during catalysis. These results demonstrate the superior stability of Ru/H-SY, reflecting the enhanced (hydro)thermal stability of high-silica zeo-

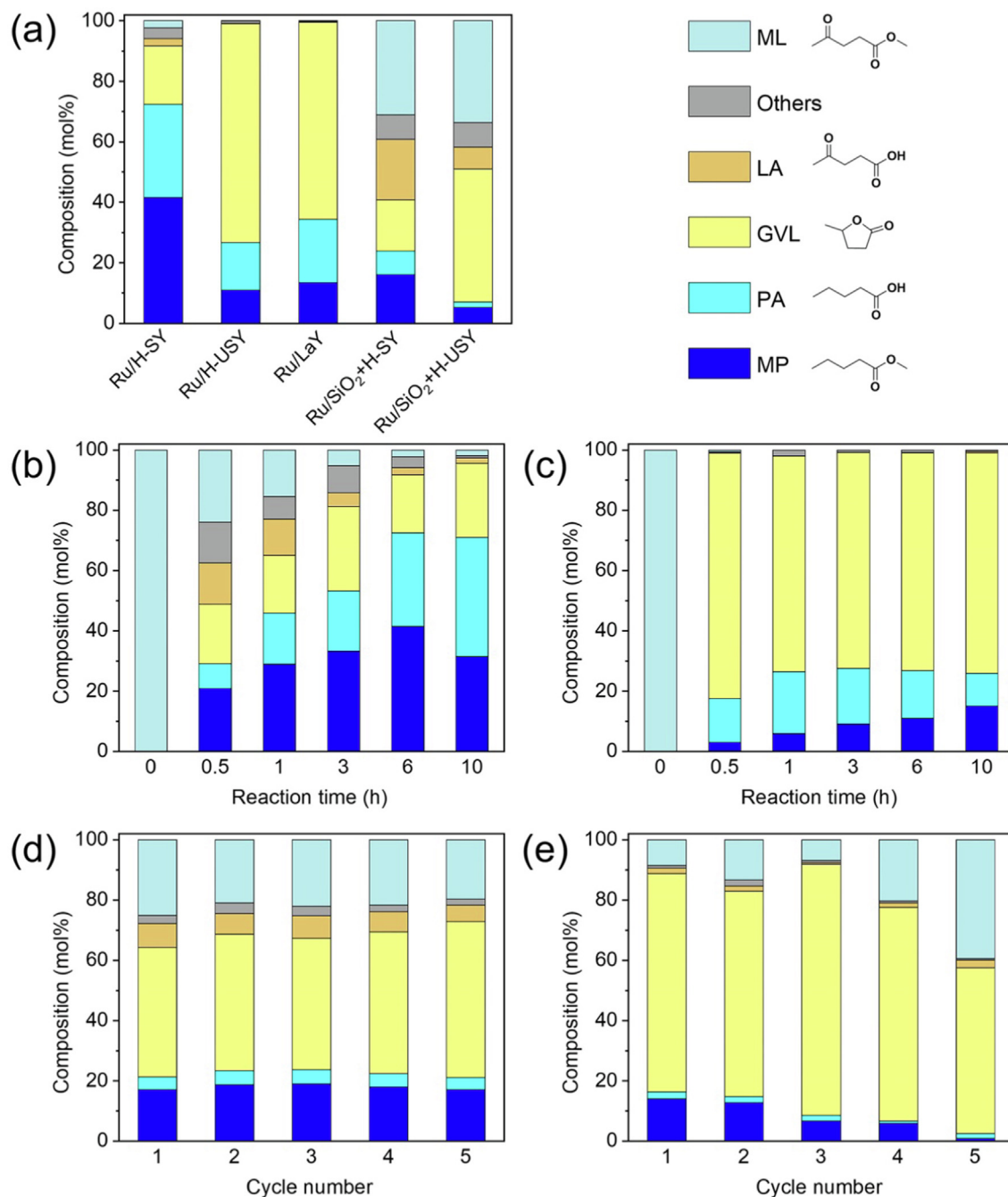


Fig. 4. (a) Catalytic performance of various bifunctional catalysts in direct HDO of ML after 6 h reaction. (b, c) Product evolution of the ML HDO over Ru/H-SY and Ru/H-USY, respectively. (d, e) Cycle evaluations of Ru/H-SY and Ru/H-USY, respectively. Reaction conditions of (a–c): 180 °C, 4 MPa H₂, mechanical stirring (1000 r min⁻¹), 10 g ML and 1 g catalyst in a 50 mL batch autoclave reactor. Reaction conditions of (d, e) were the same as (a–c) except 0.5 g catalyst with a reaction time of 30 min. ML: methyl levulinate; GVL: γ -valerolactone; LA: levulinic acid; PA: pentanoic acid; MP: methyl pentanoate.

lite Y associated with the significantly improved zeolite crystallinity.

The ‘right fit’ of the constrained environment provided by zeolite cavities is found to play an essential role in stabilization of transition states [53–56], which could be beneficial for the enhanced activity and selectivity. To unravel the insights into the superior performance of Ru/H-SY, a detailed kinetic study has been performed for the catalysts in the HDO of ML or GVL with dioxane as solvent (Fig. S12). As shown in Fig. 5, the apparent activation energy for ML conversion (E_a^{ML}) is determined to be 54 kJ mol⁻¹ for Ru/H-SY and 62 kJ mol⁻¹ for Ru/H-USY, respectively. Although

the reaction rate of ML over Ru/H-USY (with GVL as the main product) is faster than that over Ru/H-SY (Fig. 5b and c), the lower E_a^{ML} on Ru/H-SY represents a lower integrated activation barriers of the HDO of ML, likely via ML-4-HPE-MP (Route 1). Based on our previous reports, we have proposed that the notable stabilization of 4-HPE (4-hydroxypentanoic acid ester) intermediate in the constraints of zeolite cavities is essential for facilitating the production of pentanoic biofuels. The good crystallinity of high-silica zeolite Y endows the Ru/H-SY with the well-maintained micropore constraints of the FAU zeolite, which enables that the direct HDO of ML primarily undergoes Route 1 with a transition intermediate

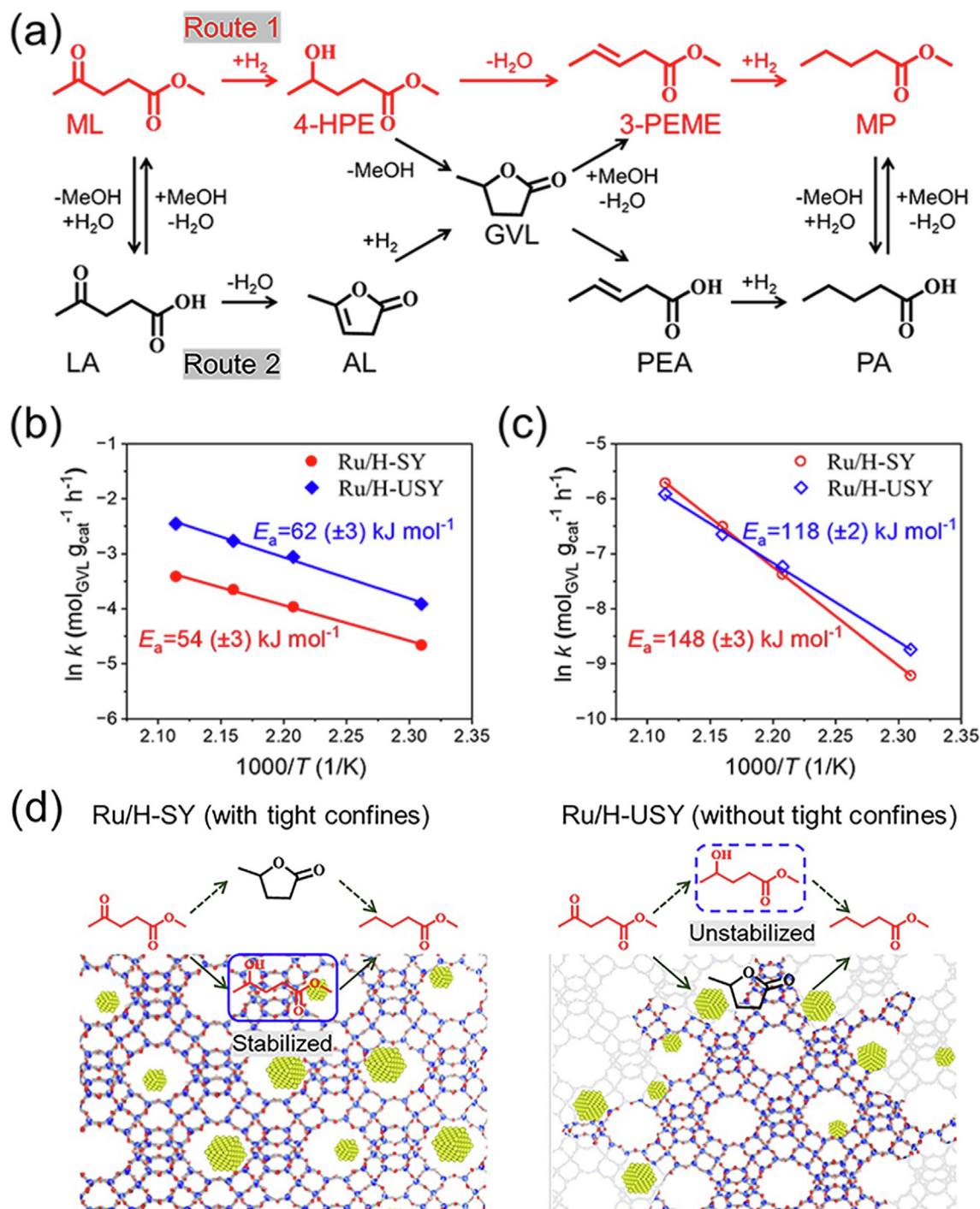


Fig. 5. (a) Possible reaction routes for the formation of pentanoic biofuels with ML as starting precursor. (b, c) Arrhenius plots for determining the apparent activation energy of ML conversion and GVL conversion on Ru/H-SY and Ru/H-USY. (d) Proposed insight into the pathway of selective HDO of ML on the catalysts. 4-HPE: 4-hydroxypentanoic acid ester; 3-PEME: 3-pentenoic acid methyl ester; AL: angelica lactone; PEA: 3-pentenoic acid; PA: pentanoic acid.

of 4-HPE. In contrast, Ru/H-USY with plenty of framework defects and mesopores, which provide an inferior constrained environment of ‘right fit’ for the transition intermediate, inevitably facilitates the direct HDO of ML proceeding via the Route 2 with GVL as the major intermediate. As shown in Fig. 5(c), the apparent activation energy for GVL hydrogenation (E_a^{GVL}) is determined to be 148 kJ mol⁻¹ for Ru/H-SY and 118 kJ mol⁻¹ for Ru/H-USY, respectively, which is much higher than E_a^{ML} , confirming that the ring-opening step of GVL is the rate-determining step in the whole reaction network of ML HDO. These results validate again the rational-

ity and feasibility of Route 1 for Ru/H-SY, which favors the lower activation barrier route via 4-HPE as the transition intermediate, rather than the higher activation barrier route via GVL as a major intermediate. Additionally, the enhanced accessibility of strong acid sites of Ru/H-SY, obtained by direct synthesis rather than dealumination treatment, could further facilitate the stabilization of reaction transition states, as tight confines in molecularly sized pores with enhanced acid functions can markedly enhance the stabilization of active/unstable transition intermediates, resembling the constraints in pockets of enzymes stabilizing active species.

Therefore, Ru/H-SY, which provides ultra-small Ru nanoclusters, enhanced accessibility of strong acid sites. The tight confinement environment with a close metal-acid site proximity can effectively stabilize transition intermediate of 4-HPE and thus allow for the enhancement of catalytic performance in the direct HDO of ML into pentanoic biofuels under mild conditions.

3. Conclusions

In summary, we have successfully developed Ru nanoclusters encapsulated in the cavities of high-silica zeolite Y with a SAR of 10 via a cooperative strategy for direct zeolite synthesis and an improved wet impregnation for metal encapsulation. The resultant Ru/H-SY catalyst possesses a close metal-acid site proximity confined inside the zeolite cavities, demonstrated by electron microscopy-based techniques, including AC-HAADF-STEM and iDPC-STEM. Compared with the benchmark hierarchical H-USY encapsulated Ru clusters, the Ru/H-SY exhibits a good integrity of the FAU structure and an enhanced accessibility of acid sites, which thus enables a previously unattained, superior performance in terms of activity, selectivity and stability in the ML HDO towards the production of pentanoic biofuels at mild reaction temperature of 180 °C. Further kinetic studies reveal that such an enhancement of catalytic reactivity is attributed to the notable stabilization of transition states by molecularly sized constraints of zeolite pores consisting of metal-acid proximity, which could thus efficiently suppress the rate determining step of GVL ring-opening. Our findings extend two key concepts of “tight confines” and “site proximity” into biomass catalysis, and such a combination of confinement and intimacy principles can be of great aid to open new opportunities for rational design of efficient bifunctional catalysts that can deliver an improved and even previously unattained performance, in analogy to enzymatic systems.

Experimental section

Experimental details can be found in the [Supporting Information](#).

Declaration of competing interest

The authors declare that they have no known competing financial interests or personal relationships that could have appeared to influence the work reported in this paper.

Acknowledgments

This work is supported by the National Natural Science Foundation of China (22288101, 21991090, 21991091, 22078316, 22272171 and 22109167) and the Sino-French International Research Network (Zeolites). We acknowledge the BL01B1 beamline of SPring-8 and the 1W1B station of Beijing Synchrotron Radiation Facility (BSRF) for the support of XAS measurements. We appreciate the Division of Energy Research Resources of Dalian Institute of Chemical Physics for the support of iDPC-STEM measurements. Dr. H. Qi acknowledges the support of the Alexander von Humboldt Foundation (CHN 1220532 HFST-P).

Appendix A. Supplementary material

Supplementary data to this article can be found online at <https://doi.org/10.1016/j.jechem.2023.10.009>.

References

- [1] P. Tian, Y.X. Wei, M. Ye, Z.M. Liu, *ACS Catal.* 5 (2015) 1922–1938.
- [2] W. Vermeiren, J.P. Gilson, *Top. Catal.* 52 (2009) 1131–1161.
- [3] P.A. Jacobs, M. Dusselier, B.F. Sels, *Angew. Chem. Int. Ed.* 53 (2014) 8621–8626.
- [4] J. Zecevic, G. Vanbutsele, K.P. de Jong, J.A. Martens, *Nature* 528 (2015) 245–254.
- [5] B.M. Weckhuysen, J.H. Yu, *Chem. Soc. Rev.* 44 (2015) 7022–7024.
- [6] D.L. Zhu, L.Y. Wang, D. Fan, N.N. Yan, S.J. Huang, S.T. Xu, P. Guo, M. Yang, J.M. Zhang, P. Tian, Z.M. Liu, *Adv. Mater.* 32 (2020) 2000272.
- [7] Q.M. Sun, N. Wang, J.H. Yu, *Adv. Mater.* 33 (2021) 2104442.
- [8] E.B. Clatworthy, S.V. Konnov, F. Dubray, N. Nesterenko, J.P. Gilson, S. Mintova, *Angew. Chem. Int. Ed.* 59 (2020) 19414–19432.
- [9] M. Gao, Z. Gong, X. Weng, W. Shang, Y. Chai, W. Dai, G. Wu, N. Guan, L. Li, *Chin. J. Catal.* 42 (2021) 1689–1699.
- [10] P. Cao, L. Lin, H.F. Qi, R. Chen, Z.J. Wu, N. Li, T. Zhang, W.H. Luo, *ACS Catal.* 11 (2021) 10246–10256.
- [11] Y.C. Chai, W.X. Shang, W.J. Li, G.J. Wu, W.L. Dai, N.J. Guan, L.D. Li, *Adv. Sci.* 6 (2019) 1900299.
- [12] L.X. Wang, L. Wang, X.J. Meng, F.S. Xiao, *Adv. Mater.* 31 (2019) 1901905.
- [13] J. He, Z.J. Wu, Q.Q. Gu, Y.S. Liu, S.Q. Chu, S.H. Chen, Y.F. Zhang, B. Yang, T.H. Chen, A.Q. Wang, B.M. Weckhuysen, T. Zhang, W.H. Luo, *Angew. Chem. Int. Ed.* 60 (2021) 23713–23721.
- [14] P. He, Q.S. Yi, H.W. Geng, Y.C. Shao, M. Liu, Z.J. Wu, W.H. Luo, Y.S. Liu, V. Valtchev, *ACS Catal.* 12 (2022) 14717–14726.
- [15] J.Q. Yang, Y. He, J.S. He, Y.S. Liu, H.W. Geng, S.H. Chen, L. Lin, M. Liu, T.H. Chen, Q.K. Jiang, B.M. Weckhuysen, W.H. Luo, Z.J. Wu, *ACS Catal.* 12 (2022) 1847–1856.
- [16] J. He, L. Lin, W.H. Luo, *ChemCatChem* 14 (2022) e202200728.
- [17] Y. Wu, S. Xi, C. Chen, Q. Hu, Z. Xiong, J. Wang, Y. Dai, Y. Han, S. Jiang, J. Wang, Y. Zhou, *Sci. Chi. Chem.* 66 (2023) 2690–2699.
- [18] Q. Zhang, W. Huang, W.H. Cui, X.Z. Dong, G.Y. Liu, Y.P. Xu, Z.M. Liu, *Mol. Catal.* 545 (2023) 113210.
- [19] X. Liu, Y. Liu, Y. Wu, S. Dong, G. Qi, C. Chen, S. Xi, P. Luo, Y. Dai, Y. Han, Y. Zhou, Y. Guo, J. Wang, *J. Hazard. Mater.* 458 (2023) 131848.
- [20] X. Liu, L. Chen, H. Xu, S. Jiang, Y. Zhou, J. Wang, *Chin. J. Catal.* 42 (2021) 994–1003.
- [21] L. Wu, J. Xin, Y. Wang, K. Zhang, J. Zhang, J. Sun, R. Zou, J. Liang, *J. Energy Chem.* 84 (2023) 363–373.
- [22] L. Xie, R. Wang, Y. Chai, X. Weng, N. Guan, L. Li, *J. Energy Chem.* 63 (2021) 262–269.
- [23] J. He, L. Lin, M. Liu, C. Miao, Z. Wu, R. Chen, S. Chen, T. Chen, Y. Su, T. Zhang, W. Luo, *J. Energy Chem.* 70 (2022) 347–355.
- [24] E.T.C. Vogt, B.M. Weckhuysen, *Chem. Soc. Rev.* 44 (2015) 7342–7370.
- [25] I. Vollmer, M.J.F. Jenks, R.M. Gonzalez, F. Meirer, B.M. Weckhuysen, *Angew. Chem. Int. Ed.* 60 (2021) 16101–16108.
- [26] Z.X. Qin, K.A. Cychosz, G. Melinte, H. El Siblani, J.P. Gilson, M. Thornmes, C. Fernandez, S. Mintova, O. Ersen, V. Valtchev, *J. Am. Chem. Soc.* 139 (2017) 17273–17276.
- [27] D. Verboekend, G. Vile, J. Perez-Ramirez, *Adv. Funct. Mater.* 22 (2012) 916–928.
- [28] T. Ennaert, J. Van Aelst, J. Dijkmans, R. De Clercq, W. Schutyser, M. Dusselier, D. Verboekend, B.F. Sels, *Chem. Soc. Rev.* 45 (2016) 584–611.
- [29] D. Kerstens, B. Smeyers, J. Van Waeyenberg, Q. Zhang, J.H. Yu, B.F. Sels, *Adv. Mater.* 32 (2020) 2004690.
- [30] D.L. Zhu, L.Y. Wang, W.N. Zhang, D. Fan, J.Z. Li, W.H. Cui, S.J. Huang, S.T. Xu, P. Tian, Z.M. Liu, *Angew. Chem. Int. Ed.* 61 (2022) e202117698.
- [31] Q.L. Ke, I. Khalil, B. Smeyers, Z. Li, R. Oliveira-Silva, B. Sels, D. Sakellariou, M. Dusselier, *Angew. Chem. Int. Ed.* 60 (2021) 24189–24197.
- [32] W.H. Luo, W.X. Cao, P.C.A. Bruijninx, L. Lin, A.Q. Wang, T. Zhang, *Green Chem.* 21 (2019) 3744–3768.
- [33] C. Mondelli, G. Gozaydin, N. Yan, J. Perez-Ramirez, *Chem. Soc. Rev.* 49 (2020) 3764–3782.
- [34] L. Yan, Q. Yao, Y. Fu, *Green Chem.* 19 (2017) 5527–5547.
- [35] J.P. Lange, R. Price, P.M. Ayoub, J. Louis, L. Petrus, L. Clarke, H. Gosselink, *Angew. Chem. Int. Ed.* 49 (2010) 4479–4483.
- [36] W.H. Luo, P.C.A. Bruijninx, B.M. Weckhuysen, *J. Catal.* 320 (2014) 33–41.
- [37] B.Y. Shen, X. Chen, H.Q. Wang, H. Xiong, E.G.T. Bosch, I. Lazić, D.L. Cai, W.Z. Qian, S.F. Jin, X. Liu, Y. Han, F. Wei, *Nature* 592 (2021) 541–544.
- [38] H. Xiong, Z.Q. Liu, X. Chen, H.Q. Wang, W.Z. Qian, C.X. Zhang, A.M. Zheng, F. Wei, *Science* 376 (2022) 491–496.
- [39] L.M. Liu, N. Wang, C.Z. Zhu, X.N. Liu, Y.H. Zhu, P. Guo, L. Alfilfil, X.L. Dong, D.L. Zhang, Y. Han, *Angew. Chem. Int. Ed.* 59 (2020) 819–825.
- [40] I. Lazić, E.G.T. Bosch, S. Lazar, *Ultramicroscopy* 160 (2016) 265–280.
- [41] C.A. Emeis, *J. Catal.* 141 (1993) 347–354.
- [42] F.J. Yi, Y.L. Chen, Z.C. Tao, C.X. Hu, X.F. Yi, A.M. Zheng, X.D. Wen, Y.F. Yun, Y. Yang, Y.W. Li, *J. Catal.* 380 (2019) 204–214.
- [43] R.X. Zhang, S.J. Xu, D. Raja, N.B. Khusni, J.M. Liu, J.Y. Zhang, S. Abdulridha, H. Xiang, S.S. Jiang, Y.N. Guan, Y.L. Jiao, X.L. Fan, *Micropor. Mesopor. Mater.* 278 (2019) 297–306.
- [44] P. Liu, Z. Li, X.Y. Liu, W.Y. Song, B.W. Peng, X.Y. Zhang, S.F. Nie, P.H. Zeng, Z.D. Zhang, X.H. Gao, B.J. Shen, *ACS Catal.* 10 (2020) 9197–9214.
- [45] W.H. Luo, M. Sankar, A.M. Beale, Q. He, C.J. Kiely, P.C.A. Bruijninx, B.M. Weckhuysen, *Nat. Commun.* 6 (2015) 6540.

- [46] Y.R. Zhang, X.L. Yang, X.F. Yang, H.M. Duan, H.F. Qi, Y. Su, B.L. Liang, H.B. Tao, B. Liu, D. Chen, X. Su, Y.Q. Huang, T. Zhang, *Nat. Commun.* 11 (2020) 3185.
- [47] Y. Kikuzono, S. Kagami, S. Naito, T. Onishi, K. Tamaru, *Faraday Discuss.* 72 (1981) 135–143.
- [48] O. Cairon, T. Chevreau, *J. Chem. Soc. Faraday Trans.* 94 (1998) 323–330.
- [49] O. Cairon, T. Chevreau, J.C. Lavalley, *J. Chem. Soc. Faraday Trans.* 94 (1998) 3039–3047.
- [50] O. Cairon, K. Thomas, T. Chevreau, *Micropor. Mesopor. Mater.* 46 (2001) 327–340.
- [51] K.I. Hadjiivanov, G.N. Vayssilov, in: *Advances in Catalysis*, Elsevier Academic Press Inc., San Diego, 2002, pp. 307–511.
- [52] Y. Wang, D.Y. Yang, S.Z. Li, M.Q. Chen, L.M. Guo, J. Zhou, *Micropor. Mesopor. Mater.* 258 (2018) 17–25.
- [53] N. Pfriem, P.H. Hintermeier, S. Eckstein, S. Kim, Q. Liu, H. Shi, L. Milakovic, Y.S. Liu, G.L. Haller, E. Barath, Y. Liu, J.A. Lercher, *Science* 372 (2021) 952–957.
- [54] Y.S. Liu, A. Vjunov, H. Shi, S. Eckstein, D.M. Camaioni, D.H. Mei, E. Barath, J.A. Lercher, *Nat. Commun.* 8 (2017) 14113.
- [55] H. Shi, S. Eckstein, A. Vjunov, D.M. Camaioni, J.A. Lercher, *Nat. Commun.* 8 (2017) 15442.
- [56] R. Gounder, E. Iglesia, *Angew. Chem. Int. Ed.* 49 (2010) 808–811.